Journal of Controlled Release 356 (2023) 554–566

Contents lists available at ScienceDirect

Journal of Controlled Release

journal homepage: www.elsevier.com/locate/jconrel

Differentiation therapy for murine myelofibrosis model with MLN8237 loaded low-density lipoproteins

Binghong He [a,1], Chao Wang [b,1], Fuping Wang [a], Liang Tian [b], Haitao Wang [c], Chunling Fu [d], Jin Liu [a], Chao Xi [a], Chunlei Zhu [b,*], Qiong Yang [a,*]

[a] Beijing Key Laboratory of Gene Resource and Molecular Development, College of Life Sciences, Beijing Normal University; Beijing 100875, China
[b] Key Laboratory of Functional Polymer Materials of Ministry of Education, State Key Laboratory of Medicinal Chemical Biology, Frontiers Science Center for New Organic Matter, College of Chemistry, Nankai University, Tianjin 300071, China
[c] Department of Hematology and Oncology, The Fourth Medical Center of the Chinese People's Liberation Army General Hospital, Beijing 100010, China
[d] Blood Disease Institute, Xuzhou Medical University, Xuzhou 221004, China

ARTICLE INFO

Keywords:
Reconstituted low-density lipoprotein
Aurora kinase A inhibitor
Differentiation therapy
Dual targeting
MPLW515L murine myelofibrosis model

ABSTRACT

Primary myelofibrosis (PMF) is a severe myeloproliferative neoplasm that is characterized by low-differentiation megakaryoblasts and progressive bone marrow fibrosis. Although an Aurora kinase A (AURKA) targeting small-molecule inhibitor MLN8237 has been approved in clinical trials for differentiation therapy of high-risk PMF patients, its off-target side effects lead to a partial remission and serious complications. Here, we report a dual-targeting therapy agent (rLDL-MLN) with great clinical translation potential for differentiation therapy of PMF disease. In particular, the reconstituted low-density lipoprotein (rLDL) nanocarrier and the loaded MLN8237 can actively target malignant hematopoietic stem/progenitor cells (HSPCs) via LDL receptors and intracellular AURKA, respectively. In contrast to free MLN8237, rLDL-MLN effectively prohibits the proliferation of PMF cell lines and abnormal HSPCs and significantly induces their differentiation, as well as prevents the formation of erythrocyte and megakaryocyte colonies from abnormal HSPCs. Surprisingly, even at a 1500-fold lower dosage (0.01 mg/kg) than that of free MLN8237, rLDL-MLN still exhibits a much more effective therapeutic effect, with the PMF mice almost clear of blast cells. More importantly, rLDL-MLN promotes hematological recovery without any toxic side effects at the effective dosage, holding great promise in the targeted differentiation therapy of PMF patients.

1. Introduction

Primary myelofibrosis (PMF) is a major subtype of myeloproliferative neoplasm and accompanied by the expansion of the atypical and poorly differentiated megakaryoblasts [1]. The low differentiation and immature megakaryoblasts are closely associated with progressive bone marrow fibrosis and extramedullary hematopoiesis during the development of PMF [2,3]. Small molecule inhibitors targeting overactivated JAK/STAT signaling in megakaryoblasts have long been investigated to improve the PMF symptom, in which the JAK2 inhibitor ruxolitinib has been approved for clinical treatment [1]. Although ruxolitinib gives rise to symptomatic relief, it does not reduce the mutant allele burden and is prone to be intolerant for some patients [4]. In this regard, the agents targeting Aurora kinase A (AURKA) immature megakaryocytes have been developed to ameliorate fibrosis and extramedullary hematopoiesis of PMF [3,5]. In general, AURKA is overexpressed and constitutively activated in the abnormal megakaryocytes, which plays a critical role in promoting cell proliferation and inhibiting cell polyploidization and differentiation [5,6]. We previously reported that AURKA was an effective therapeutic target in PMF because it involves in the processes of downregulating hematopoietic transcription factor GATA1, upregulating c-MYC and p-AKT expression, and interrupting the megakaryocyte endomitosis in PMF cells [3,5,7]. Moreover, AURKA inhibition leads to an increased differentiation and subsequent apoptosis of malignant megakaryocytes in animal models of myelofibrosis and acute megakaryoblastic leukemia [5]. A genetic study demonstrated that the deletion of one allele of AURKA can effectively ameliorate fibrosis and other PMF symptoms in vivo [3]. AURKA-targeting small molecule

* Corresponding authors.
E-mail addresses: chunlei.zhu@nankai.edu.cn (C. Zhu), yangqiong@bnu.edu.cn (Q. Yang).
[1] These authors contributed equally: Binghong He, Chao Wang

https://doi.org/10.1016/j.jconrel.2023.03.024
Received 28 November 2022; Received in revised form 22 February 2023; Accepted 13 March 2023
Available online 17 March 2023
0168-3659/© 2023 Elsevier B.V. All rights reserved.

inhibitor Alisertib (MLN8237) has been proven to be an effective agent for the therapy of PMF [3,5]. Preclinical studies demonstrated that MLN8237 can significantly induce the differentiation and maturation of megakaryocytes and alleviate fibrosis when combined with the other targeted inhibitor ruxolitinib [3,5].

Although the small molecule inhibitor of AURKA showed treatment benefits to PMF patients, it did not fully attenuate the splenomegaly symptom and brought in serious complications such as anemia, neutropenia, and thrombocytopenia [8]. The limited efficiency and toxic effects are presumably caused by the off-target distribution and low bioavailability of MLN8237 in vivo. To improve its therapeutic efficiency and address its adverse effects, it is preferred to use a natural drug delivery system that is able to specifically transport MLN8237 to the malignant PMF cells in vivo. In this regard, low-density lipoprotein (LDL) is an ideal endogenous nanocarrier in view of its biocompatibility and biodegradability, reduced immunogenicity, and natural tumor-targeting capability [9]. In particular, Zhu et al. reported the use of a mixture of eutectic fatty acids to reconstitute the hydrophobic core of native LDL and obtain reconstituted LDL (rLDL) for selective killing of cancer cells [10,11]. Typically, rLDL nanoparticles enter cells through the LDL receptor (LDLR) mediated endocytosis; after endolysosomal escape, the loaded drugs are released to the cytoplasm of the malignant cells [12].

Given the strong inhibitory effect of MLN8237 on AURKA activity and the selective recognition of rLDL nanocarrier toward LDLR, we assumed that the combination of MLN8237 and rLDL could target both the LDLR-overexpressed malignant PMF cells and their intracellular AURKA, which would effectively induce the differentiation of PMF cells and inhibit their proliferation without undesirable side effects in vivo. Here, we reported a MLN8237-loaded biological nano-delivery system rLDL-MLN, in which MLN8237 was reconstituted to the hydrophobic core of LDL with the assistance of a mixture of eutectic fatty acids. Next, the dual targeting capability of rLDL-MLN to AURKA and PMF malignant cells was evaluated. Furthermore, we explored the effects of rLDL-MLN on the proliferative inhibition and differentiation induction of PMF cells with MPLW515L or JAK2V617F mutation and primary malignant hematopoietic stem/progenitor cell (HSPC). In addition, the effects of rLDL-MLN on myeloid and megakaryocyte colony formation are analyzed in MPLW515L-expressing bone marrow progenitor cells. After assessing the toxicity on tissue and hematopoietic function of healthy mice, we systematically investigated the efficacy of differentiation therapy of rLDL-MLN as well as its impact on hematologic recovery and reconstruction in the MPLW515L murine myelofibrosis model.

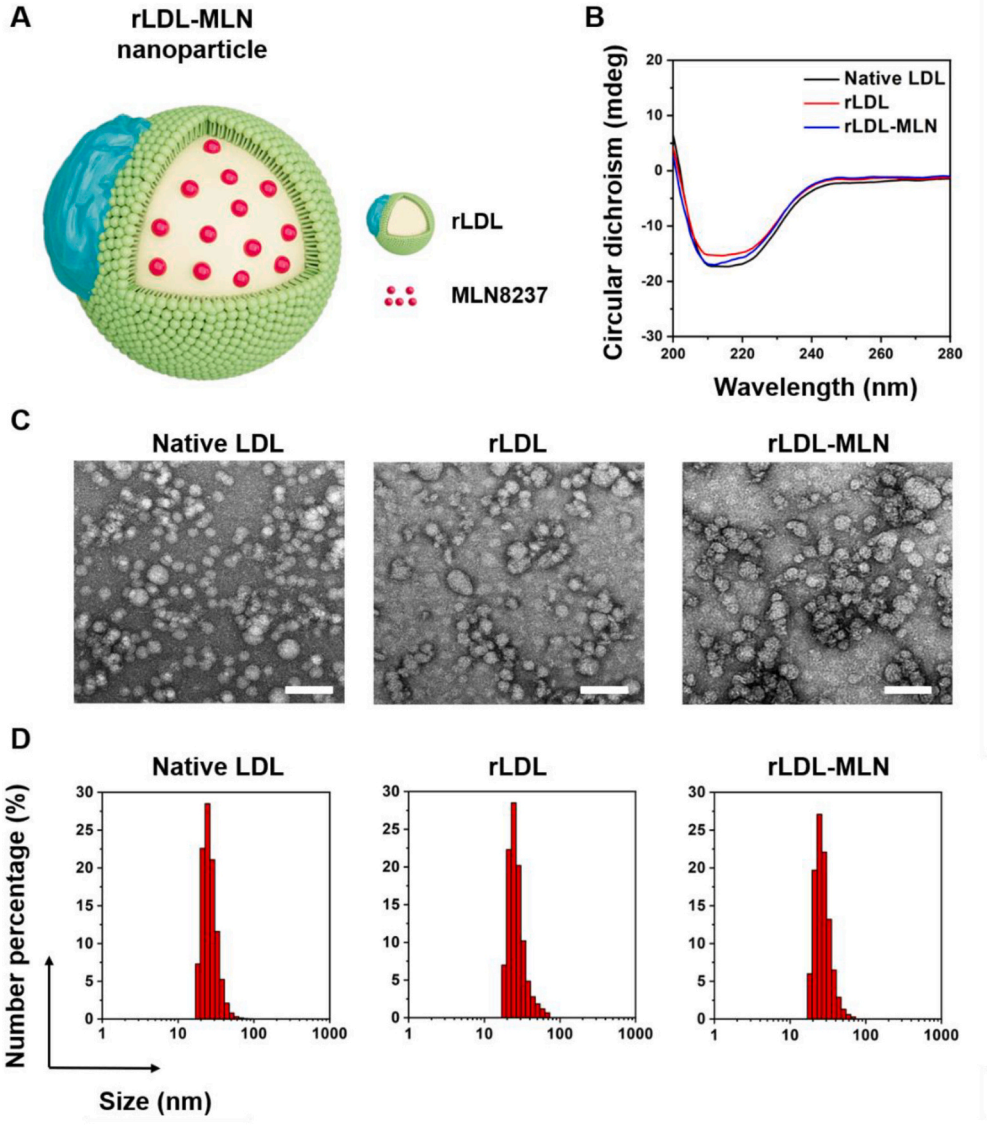

Fig. 1. Characterization of rLDL-MLN nanoparticles. (A) Schematic illustration showing the structure of rLDL-MLN, where MLN8237 is encapsulated in the eutectic mixture of lauric acid and stearic acid. (B) Circular dichroism spectra of native LDL, rLDL (without MLN8237), and rLDL-MLN, showing the characteristic negative absorption of apolipoprotein B-100 at ca. 210 nm (predominance in α-helix). (C) TEM images of native LDL, rLDL, and rLDL-MLN. Scale bars: 100 nm. (D) DLS analysis of native LDL, rLDL, and rLDL-MLN.

2. Results

2.1. Preparation of rLDL-MLN nanoparticles

First of all, we reconstituted native LDL with the small molecule inhibitor MLN8237 using our previously established core-loading strategy [10], where a eutectic mixture of lauric acid and stearic acid was employed as the loading matrix to carry MLN8237 into the core of LDL (Fig. 1A). The optimal weight ratio of MLN: lauric acid: stearic acid was determined to be 1:32:8. Transmission electron microscopy (TEM) images showed that rLDL-MLN had good dispersity and uniformity with its morphology similar to native LDL (Fig. 1C), and the diameter of rLDL-MLN was distributed at ca. 20–40 nm (Fig. S1A), which was basically consistent with the results from the dynamic light scattering (DLS) analysis (Fig. 1D). Circular dichroism spectroscopy analysis indicated that rLDL-MLN had an apolipoprotein B-100 (ApoB-100)-specific absorption peak at ca. 210 nm (Fig. 1B). In particular, each native LDL has one molecule of ApoB-100, which mediates the specific binding with LDLR in target cells via ligand-receptor interactions. The internalized rLDL-MLN is subsequently disintegrated under low pH conditions in endolysosomes, leading to the release of the small molecule inhibitor into the cytoplasm [10].

2.2. Dual targeting of rLDL-MLN to AURKA and target cells

We previously reported that MLN8237 was a potent small molecule inhibitor to AURKA [5], which is currently under preclinical trials for PMF patients [8]. To investigate the targeting capability of rLDL-MLN on megakaryoblasts, we evaluated its inhibitory effect on AURKA and selectivity to cells with different levels of LDLR. First of all, we explored the kinase-targeting function of rLDL-MLN. Western blot assay showed that rLDL-MLN downregulated the phosphate-AURKA level at the T288 site with a similar inhibitory effect as equivalent free MLN in cultured cells (Fig. 2A). It is well known that LDLR expression is elevated in proliferating leukemia cells [13] and other cancer cells [10]. Our data demonstrated that the malignant blast cells overexpressed LDLR in PMF to meet the demand of rapid cell proliferation (Fig. S2A—B). To validate the selectivity of rLDL-MLN toward leukemia cells, we screened and identified two cell lines with significantly different levels of LDLR expression, that is, K562 cells and MEG-01 cells. Both cell lines were derived from chronic myelogenous leukemia, where K562 cells have a significantly higher level of LDLR expression than that of MEG-01 (Fig. 2B). As expected, when treated with rLDL-MLN, K562 cells displayed a lower IC50 value (i.e., 68 nM) when compared to that of MEG-01 cells (128 nM) (Fig. 2C). In terms of evaluating differentiation therapy, polyploidization and the levels of megakaryocytic surface marker expression are the key parameters. At a dose of 300 nM, rLDL-MLN induced 52.9 ± 4.56% of polyploid K562 cells, where only 22.63 ± 3.76% of MEG-01 cells were subjected to polyploidization (Fig. 2D). Meanwhile, CD42 (a late marker of the megakaryocytic differentiation) in K562 cells treated with rLDL-MLN significantly elevated when compared to MEG-01 cells (Fig. 2E). In addition, in contrast to rLDL and free MLN, rLDL-MLN showed pronounced proliferation inhibition and differentiation induction in K562 cells (Fig. S3A—F). The selective recognition and interaction of rLDL with LDLR have been confirmed in our prior study [10]. These results suggested that rLDL-MLN could impose a selective impact on LDLR-overexpressed malignant cells.

2.3. Proliferation inhibition and differentiation induction of rLDL-MLN on PMF cells

We further investigated the differentiation therapy effects of rLDL-

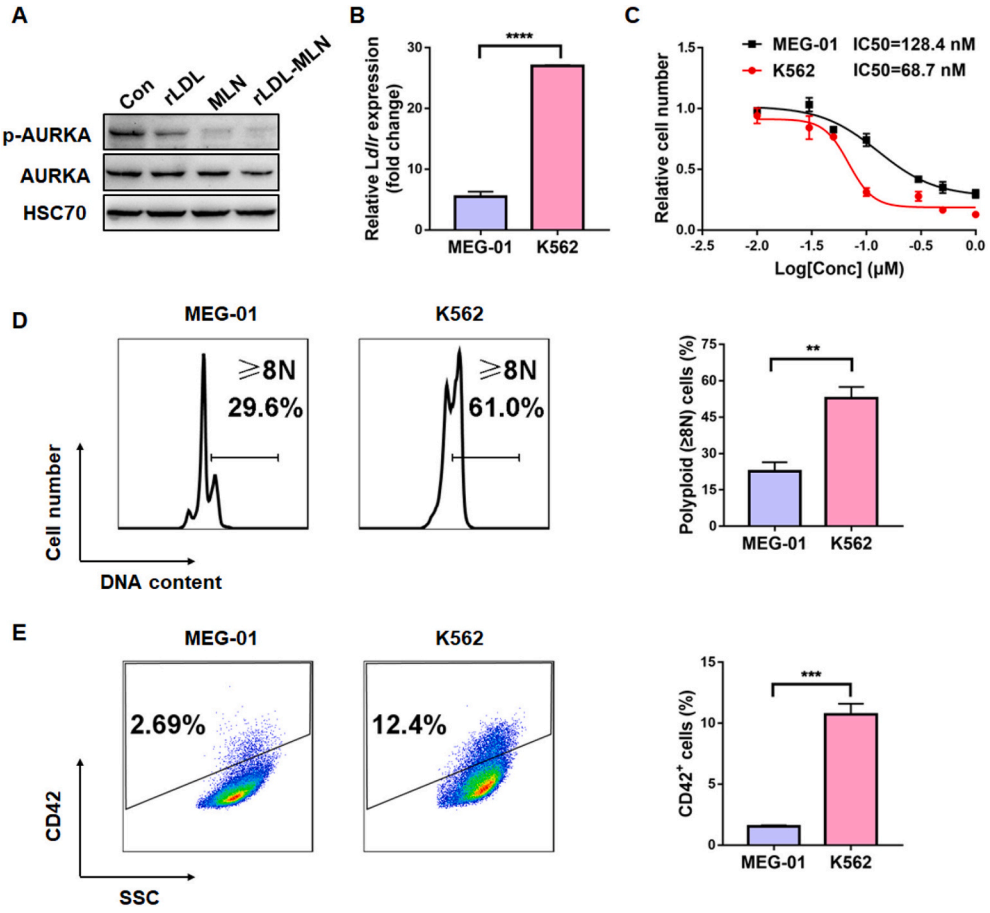

Fig. 2. Dual targeting of rLDL-MLN in leukemia cells. (A) Western blotting in HEL cells for analysis of AURKA kinase inhibition by rLDL-MLN. The cells were treated with rLDL, MLN, or rLDL-MLN at 30 nM or tricine for 6 h. The expression of phospho-AURKA and total AURKA was detected with HSC70 as a loading control. (B) The expression of *Ldlr* mRNA in K562 and MEG-01 cells by qPCR. β-actin served as the internal control. (C) The proliferation curves and IC50 values of K562 and MEG-01 cells treated with rLDL-MLN. The cells were treated with ascending concentrations of rLDL-MLN (1–1000 nM) for 48 h. Growth of the drug-treated cells was normalized to that of cells treated with tricine, and IC50 was calculated by nonlinear regression analysis using GraphPad Prism. (D) Flow cytometry for the analysis of the polyploidization of K562 and MEG-01 cells. (E) Flow cytometry for the analysis of CD42 expression on the surface of K562 and MEG-01 cells. In terms of the polyploidization and CD42 expression analysis, K562 and MEG-01 cells were treated with rLDL-MLN at 300 nM for 72 h. Representative flow cytometry plots (left) and quantification (right) of cells showing DNA content or CD42 expression. Bar graphs depicting the mean ± SEM of three independent experiments, $^{**}P < 0.01$, $^{***}P < 0.005$, $^{****}P < 0.001$, compared between K562 and MEG-01 cells by the unpaired two-sided Student's *t*-test.

MLN on PMF cells. The 6133/MPLW515L cell line was used for in vitro assay since it harbors PMF-driven MPLW515L mutation and possesses megakaryocytic differentiation potential [5]. In contrast to the wildtype control, 6133/MPLW515L cells had a significantly higher level of LDLR expression (Fig. S2C), and rLDL-MLN should exhibit stronger proliferation inhibition. As expected, the IC50 values for rLDL-MLN and MLN at 24 h were 17.8 nM and 42.3 nM, respectively (Fig. 3A). At 72 h post treatment, the IC50 for rLDL-MLN was down to 7.6 nM, whereas the IC50 for free MLN was 35.2 nM (Fig. 3B). Surprisingly, in contrast to equivalent free MLN, rLDL-MLN treatment resulted in remarkably enhanced proliferation arrest (Fig. 3C) and apoptosis induction (Fig. 3D). The megakaryocytic differentiation biomarker CD41 (a marker of the megakaryocytic lineage) also significantly upregulated at 72 h post rLDL-MLN treatment when compared to free MLN, rLDL, and tricine control (Fig. 3E). Meanwhile, we also observed the larger cells with multiple nucleus for the group treated with rLDL-MLN under the microscope (Fig. 3F). At a dose of 50 nM, rLDL-MLN induced 45.37 ± 1.98% of polyploid cells, where the value was only 22.37 ± 0.55% for

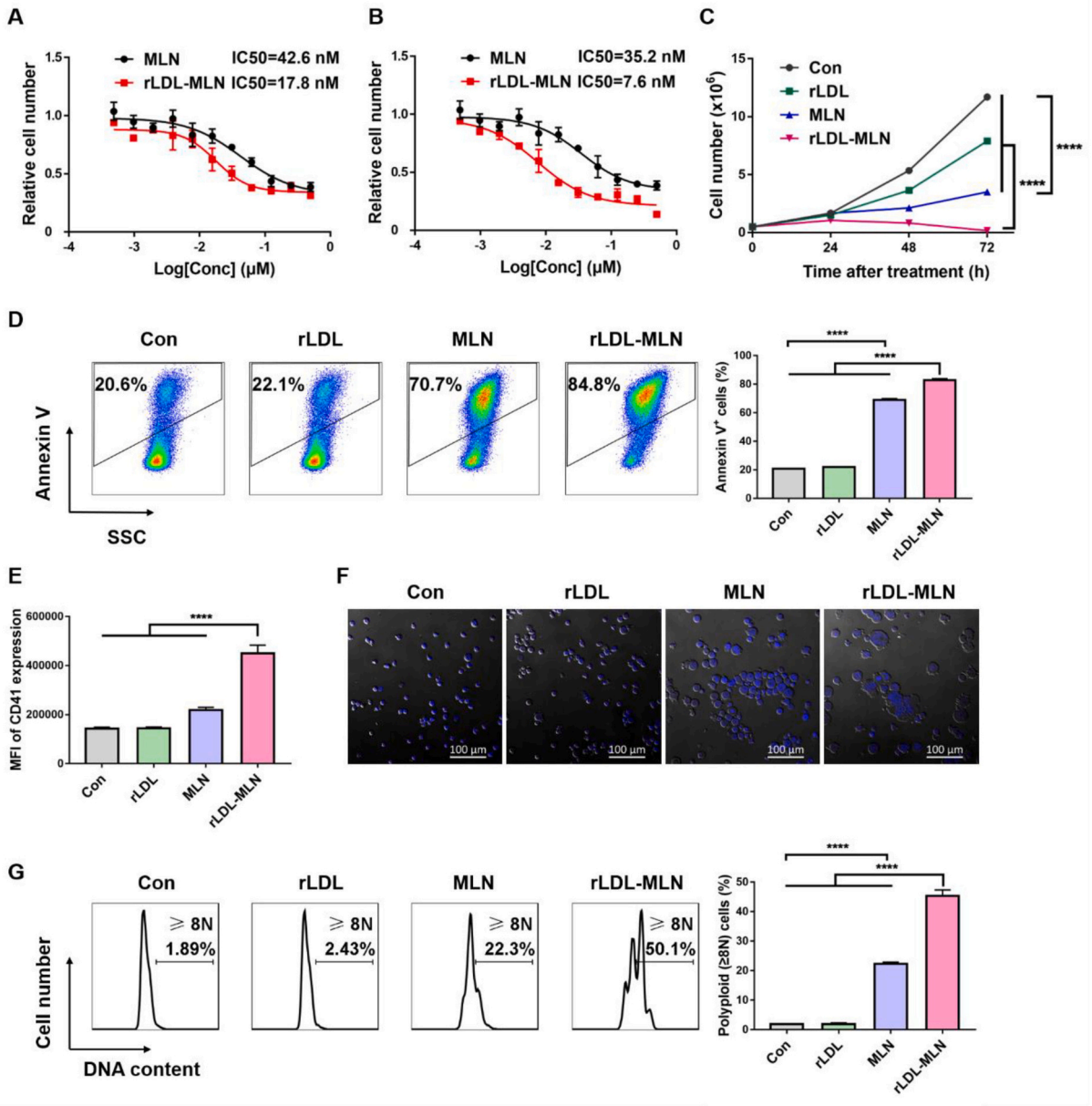

Fig. 3. Proliferation inhibition and differentiation induction of rLDL-MLN on 6133/MPLW515L cells. (A) The proliferation curves and IC50 values of 6133/MPLW515L cells treated with rLDL-MLN or MLN for 24 h. (B) The proliferation curves and IC50 values of 6133/MPLW515L cells treated with rLDL-MLN or MLN for 72 h. The cells were treated with ascending concentrations (0.5–500 nM) of rLDL-MLN or MLN for 24 h and 72 h. IC50 was calculated with non-linear regression analysis of GraphPad Prism 7.0 software. (C) The absolute numbers of the induced 6133/MPLW515L cells. (D) Flow cytometry for the analysis of the apoptosis of the induced 6133/MPLW515L cells. The cells were stained with PE-Annexin V. Representative flow cytometry plots (left) and quantification (right) of cells showing Annexin V expression. (E) Flow cytometry for the analysis of the differentiation marker CD41 expression on the surface of the induced 6133/MPLW515L cells. MFI, mean fluorescence intensity. (F) Representative fluorescence images of the induced 6133/MPLW515L cell polyploidization. The nuclei were stained with Hoechst 33342 and is shown in blue. Scale bars: 100 μm. (G) Flow cytometry for the analysis of the polyploidization of the induced 6133/MPLW515L cells. Representative flow cytometry plots (left) and quantification (right) of the DNA content of the 6133/MPLW515L cells. For the proliferation and differentiation evaluation (C-G), these 6133/MPLW515L cells were treated with rLDL, MLN, or rLDL-MLN at 50 nM for 72 h, with tricine as the control (Con). Bar graphs depicting the mean ± SEM of three independent experiments. Statistical significance was calculated via two-way ANOVA (C) or one-way ANOVA with a Tukey post-hoc test (D, E, G). ****$P <$ 0.0001. (For interpretation of the references to color in this figure legend, the reader is referred to the web version of this article.)

free MLN (Fig. 3G).

We also evaluated the differentiation induction benefits in SET-2 and HEL cell lines harboring JAK2V617F mutation, which is the most frequent mutation of PMF patients and responds to AURKA kinase inhibitor MLN8237 [14]. Our data showed that rLDL-MLN significantly induced megakaryocytic differentiation and inhibited cell proliferation in these two cell lines when compared to MLN and other controls (Fig. S4A-F and Fig. S5A-G). SET-2 and HEL cells carry heterogeneous and homogeneous JAK2V617F mutations, respectively [15]. In view of the dosage of gene mutation, SET-2 cells express more LDLR than HEL cells (Fig. S2D). As a result, the response of SET-2 cells to rLDL-MLN was much stronger than that of HEL cells (Fig. S4A-F and Fig. S5A-G), which suggested that the specific interaction between LDLR and rLDL-MLN contributed to the enhanced uptake of MLN.

To validate the effects of rLDL-MLN on primary PMF progenitor cells, bone marrow-derived c-Kit$^+$ progenitor cells carrying MPLW515L mutation were used as the model cell lines, where these primary cells were obtained by transducing Migr1-GFP-MPLW515L retrovirus. To keep the stem cell function of primary cells and mimic the in vivo real environment, we performed in vitro experiments when the c-Kit$^+$ cells were transduced with MPLW515L retrovirus for 24 h. Flow cytometry data showed that rLDL-MLN showed significant proliferation inhibition on GFP$^+$ (MPLW515L-expressing) cells when compared with MLN and other controls (Fig. 4A). It is noteworthy that the MPLW515L-expressing progenitor cells were reverted to the higher differentiation ones post treatment with rLDL-MLN, where MPLW515L-expressing progenitor cells were induced toward megakaryocytic differentiation with elevated polyploidization (Fig. 4B) and CD41 expression (Fig. 4C), indicating the advantage of rLDL-MLN in targeting and reverting malignant progenitor cells.

Furthermore, we investigated the effect of rLDL-MLN on myeloid and megakaryocyte colony formation derived from the cultured MPLW515L-expressing bone marrow progenitor cells. Our data showed that the colony-forming unit-megakaryocyte (CFU-MK) post rLDL-MLN

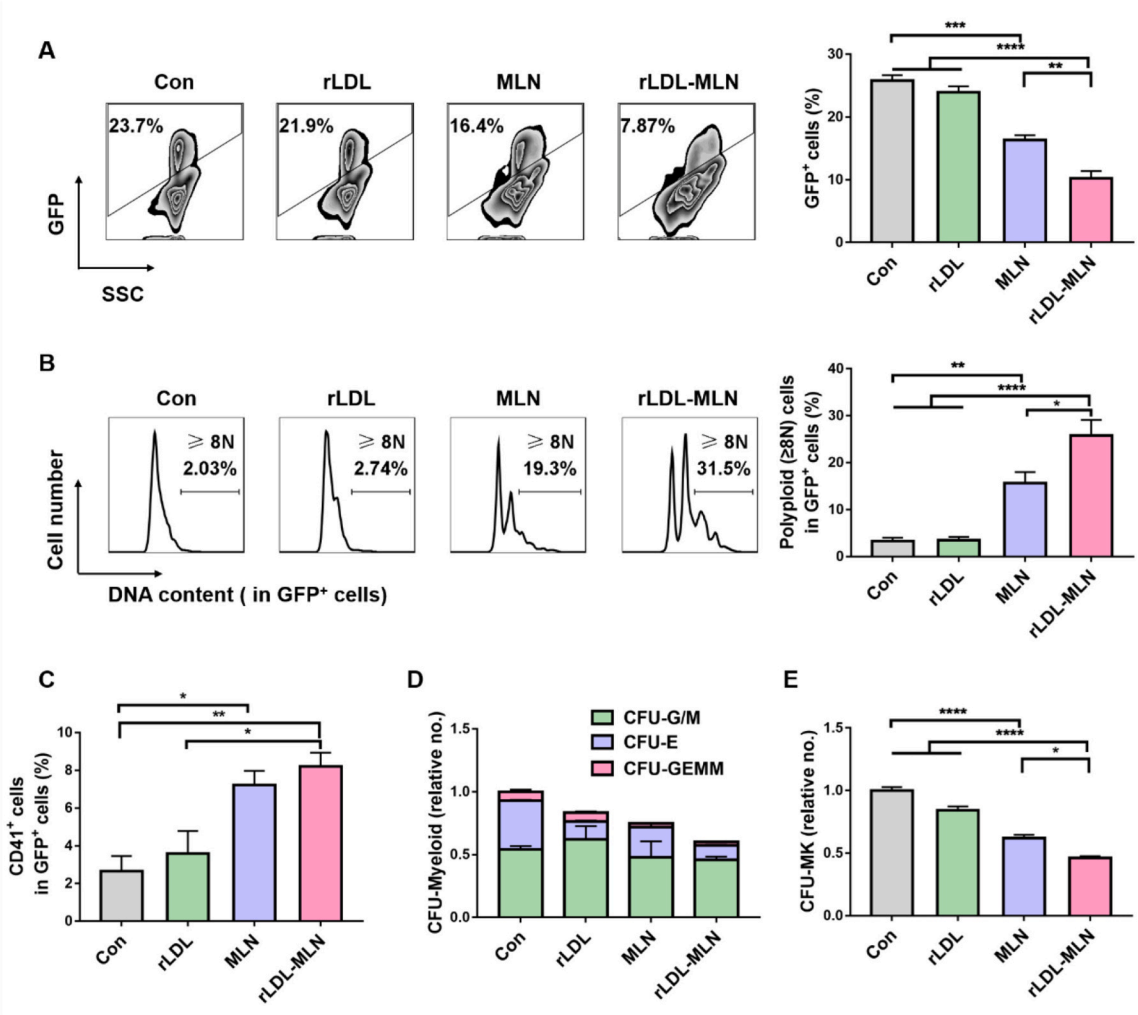

Fig. 4. Proliferation inhibition and differentiation induction of rLDL-MLN on MPLW515L-expressing bone marrow progenitor cells. Mouse bone marrow-derived c-Kit positive progenitor cells were transduced with Migr1-GFP-MPLW515L retrovirus and cultured with rLDL, MLN, or rLDL-MLN for 48 h. GFP$^+$ cells represent MPLW515L-expressing cells. (A) Flow cytometry for the analysis of the GFP percentages of the induced bone marrow progenitor cells. (B) Flow cytometry for the analysis of the polyploidization of GFP$^+$ cells of the induced bone marrow progenitor cells. Representative flow cytometry plots (left) and quantification (right) of the GFP$^+$ expression and DNA content of the induced bone marrow cells. (C) Flow cytometry for the analysis of the CD41 expression of GFP$^+$ cells of the induced bone marrow progenitor cells. (D) Colony forming unit assay of myeloid (CFU-Myeloid) of GFP$^+$ cells of the induced bone marrow progenitor cells. CFU-Myeloid includes the colony-forming unit-granulocyte-macrophage cells (CFU-G/M), colony-forming unit-erythroid (CFU-E), and colony-forming unit-multipotential granulocyte, erythroid, macrophage, megakaryocyte progenitor cells (CFU-GEMM). (E) Colony forming unit of Megakaryocytes (CFU-MK) of GFP$^+$ cells of the induced bone marrow progenitor cells in the presence of Thrombopoietin. For viability and differentiation evaluation (A-C), bone marrow progenitor cells were treated with rLDL, MLN, or rLDL-MLN at 300 nM for 48 h, with tricine as the control. Bar graphs depicting the mean ± SEM of three independent experiments. Statistical significance was calculated via one-way ANOVA with a Tukey post-hoc test (D, E). $^*P < 0.05$, $^{**}P < 0.01$, $^{***}P < 0.001$, $^{****}P < 0.0001$.

treatment was significantly decreased when compared to other control treatments (Fig. 4E). The colony-forming unit-myeloid (CFU-Myeloid) assay indicates the proliferation and differentiation ability of individual cells into erythroid (E), granulocyte/macrophage (G/M) and multipotential granulocyte, erythroid, macrophage, and megakaryocyte progenitor cells (GEMM) (Fig. 4D). Among CFU-Myeloid, the colony-forming unit-erythroid (CFU-E) post rLDL-MLN treatment showed more pronounced decrease than that of free MLN ($P = 0.0028$ vs. MLN) (Fig. S6A). However, only slight changes were found for the colony-forming unit-granulocyte-macrophage cells (CFU-G/M) and colony-forming unit-multipotential granulocyte, erythroid, macrophage, megakaryocyte progenitor cells (CFU-GEMM) (Fig. S6B—C). These results indicated that rLDL-MLN preferably affected the malignant megakaryocytic and erythroid progenitor cells, which is critical to for treatment of PMF.

2.4. Toxicity evaluation of rLDL-MLN on tissue and hematopoietic function in healthy mice

To evaluate the in vivo biosafety of rLDL-MLN, healthy C57BL/6 N mice were subjected to intravenous injection of 0.01 mg/kg rLDL-MLN, MLN, rLDL, or vehicle every other day during the 15 days observation period. No evident toxic effects on mouse tissues and hematological functions were observed for all groups. The body weight, spleen, and liver weight stayed stable during the observation period (Fig. 5A-C). The complete blood counts showed that the numbers of white blood cells (WBC), red blood cell (RBC), and platelets and hemoglobin (HGB) values were all within normal physiological ranges upon different treatments (Fig. 5E-H). The percentages of mature granulocytes, erythroid progenitor cells, and megakaryocytes of the bone marrow (Fig. 5I-K) and spleen (Fig. 5L-N) were basically not influenced post treatment with rLDL, MLN, or rLDL-MLN. Histological staining of the liver, spleen, bone marrow, and blood smears in the rLDL-MLN-treated group did not show observable changes when compared to the vehicle control (Fig. 5D).

2.5. Relief of the PMF disease by rLDL-MLN via inducing megakaryocytic differentiation in the murine myelofibrosis model

After confirming the biosafety of rLDL-MLN in vivo, we evaluated its efficacy of the differentiation therapy in the MPLW515L murine myelofibrosis model. Such a model shows typical pathological features and symptoms, such as poorly differentiated and immature megakaryocytic blasts, bone marrow, and spleen fibrosis [3]. In contrast to healthy individuals, both bone marrow and spleen cells in the PMF mice exhibit elevated LDLR expression (Fig. S2E—F). Surprisingly, even at an extremely low dosage of rLDL-MLN (0.01 mg/kg), the symptoms of the PMF mice were remarkably relieved symptoms with almost complete recovery. It is noteworthy that the effective dosage of rLDL-MLN (0.01 mg/kg) is far lower than that of MLN8237 (15–30 mg/kg) as demonstrated in our previous report [3]. In particular, the treatment of rLDL-MLN nearly cleared the MPLW515L-bearing malignant cells in the blood (Fig. 6A, Fig. S7H), bone marrow (Fig. 6B), and spleen (Fig. 6C), whereas the equivalent MLN-treated mice still had 30% of the malignant cells. In contrast, the vehicle-treated mice developed an aggressive PMF, with the malignant blast cells accounting for 44.8 ± 14.02% (Fig. 6A) in the peripheral blood at four-week post transplantation; under similar treatment conditions, the percentage of the malignant cells in the rLDL-treated group reached 23.82 ± 15.42%.

Our data demonstrated that rLDL-MLN treatment could effectively decrease the number of blood cell lineages and alleviate abnormal hematopoiesis in PMF murine model. Complete blood count data showed that the numbers of white blood cells and platelets in the rLDL-MLN group significantly decreased when compared to free MLN, rLDL, and the vehicle control during the entire therapeutic period (Fig. 6D-E), where the vehicle-treated mice went through myelofibrosis (Fig. 6D and K) with cytopenia. Besides, the hematocrit level and hemoglobin concentration in the rLDL-MLN treated group were slightly decreased compared to the vehicle treated mice (Fig. S7B—C). As for the rLDL-MLN-treated PMF mice, the hepatomegaly and splenomegaly were relieved (Fig. 6J, Fig. S8A—C), and the total cell numbers and mass of bone marrow and spleen significantly decreased when compared to free MLN, rLDL, and the vehicle control (Fig. S7D, S8D).

Reverting the atypical PMF megakaryocytic blast cells to normal mature ones was one of the most important effects of rLDL-MLN. Our findings demonstrated that the GFP^+ bone marrow and spleen cells isolated from the rLDL-MLN group exhibited significant increase in the $CD41^+$ cell percentage when compared to free MLN and the vehicle control (Fig. 6F, H). The polyploidization in the rLDL-MLN group was much higher than that in all the other groups treatments, with 60% of the $CD41^+$ in the GFP^+ malignant cells of the bone marrow and spleen cells (Fig. 6G, I).

Histopathological analysis showed rLDL-MLN treatment suppressed the proliferation of PMF blast cells and alleviated pathological fibrosis. There were few atypical low-polyploidy cells in the bone marrow and spleen, and the spleen and sternum in the rLDL-MLN group showed a weaker level of reticulin staining than all the other groups (Fig. 6K), indicating that rLDL-MLN could effectively prevent fibrosis formation in the PMF murine model. In addition, the fibrosis-related inflammatory cytokine TGF-β was decreased in the spleen of rLDL-MLN/MLN treated mice (Fig. S8H). Given the pivotal role of eliminating abnormal progenitor cells for the effective therapy of the PMF and leukemia disease, we investigated the effects of rLDL-MLN on the PMF progenitors and cell lineages in the PMF murine model. Flow cytometry data demonstrated that the absolute numbers of malignant GFP^+ $Lineage^-Sca\text{-}1^+c\text{-}Kit^+$ (LSK) stem cells, common-myeloid progenitor (CMP) cells, megakaryocyte-erythrocyte progenitor (MEP) cells, and granulocyte-macrophage progenitor (GMP) cells were all significantly reduced in bone marrow and spleen (Table 1, Fig. S7G, S8G) when compared to all the other groups. In addition, in the rLDL-MLN group, erythroid cells showed a higher differentiation potential and the pro-erythroid cell population ($CD71^{high}Ter119^+$) was decreased (Fig. S7E, S8E). In contrast, the percentage of $Gr1^+Mac1^+GFP^+$ granular cells was slightly elevated in the bone marrow and moderately elevated in the spleen when compared to the vehicle control (Fig. S7F, S8F), indicating the primary impacts of rLDL-MLN on the progenitor cells of megakaryocytic and erythroid cell lineages rather than granular lineage.

2.6. The role rLDL-MLN in promoting central hematopoietic recovery and reconstruction in the PMF murine model

The hematopoietic recovery and reconstruction of PMF patients are difficult due to the myelofibrosis of bone marrow and spleen. Surprisingly, the PMF mice treated with rLDL-MLN showed obvious hematopoietic recovery and reconstruction. The flow cytometry analysis indicated that the GFP^+ cell population in the bone marrow and spleen post rLDL-MLN treatment nearly disappeared (Fig. 6B, C). To further evaluate the hematopoietic status, we analyzed the differentiation pattern of GFP negative cells (without MPLW515L mutation) from the bone marrow and spleen (Fig. 7A). In central hematopoietic organ bone marrow, the myeloid progenitor ($Lineage^-Sca\text{-}1^-c\text{-}Kit^+$, LSK) in the rLDL-MLN group was significantly increased when compared to MLN, rLDL, and the vehicle control (Fig. 7B). In peripheral hematopoietic organ spleen, LSK number was moderately increased when compared with the controls (Fig. 7D). Such a finding indicated that rLDL-MLN could promote the normal hematopoietic progenitors to recover and settle in the bone marrow as well as reduce extramedullary hematopoiesis.

Furthermore, we confirmed the differentiation potential of bone marrow LSK, where rLDL-MLN treatment resulted in significantly increased GMP, CMP, and MEP in bone marrow when compared to the controls. In particular, the MEP population in the rLDL-MLN-treated mice was even comparable to that in healthy mice (Fig. 7C). In

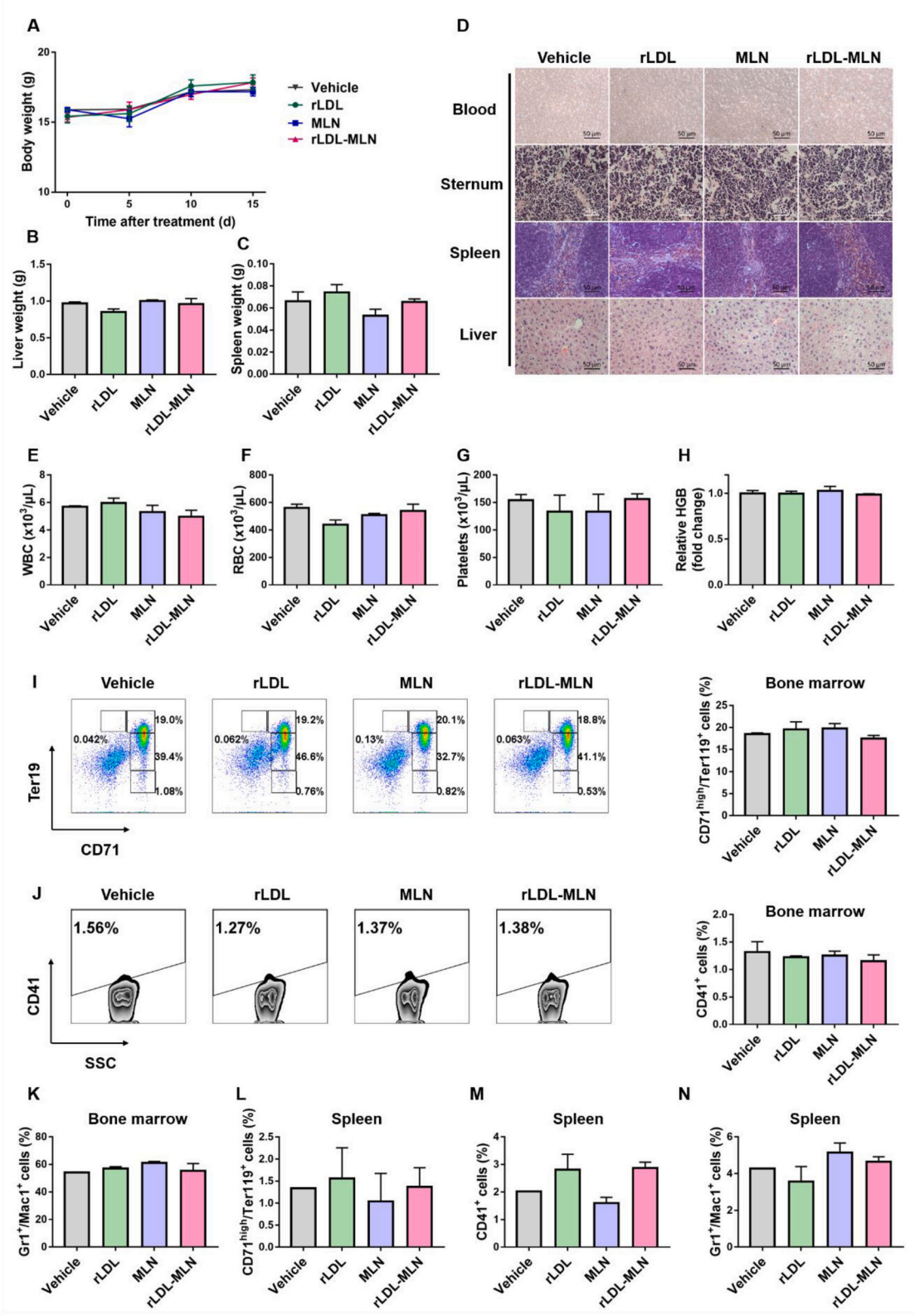

Fig. 5. Biosafety of rLDL-MLN to the cells and tissues of hematopoiesis in healthy mice. Eight-week-old healthy C57BL/6 N mice were intravenously administered with rLDL, MLN, and rLDL-MLN at 0.01 mg/kg or vehicle (tricine) for 15 days. (A) Body weights. (B) Spleen weights. (C) Liver weights. (D) Histopathological analysis of blood smears and tissue sections of bone marrow, liver, and spleen. The blood cells were Giemsa-stained, and the tissue samples were hematoxylin-eosin stained. Images were obtained with a microscope (Axio observer Z1) at a magnification of 400 ×. Scale bars: 50 μm. (E) WBC counts. (F) RBC counts. (G) Platelet counts. (H) Relative hemoglobin (HGB). (I—K) Flow cytometry for the analysis of the percentages of the erythroid ($CD71^{high}Ter119^{+}$), megakaryocytic ($CD41^{+}$), and granulocyte ($Gr1^{+}Mac1^{+}$) lineages of bone marrow post treatments. Representative flow cytometry plots (left) and quantification (right) of the $CD71^{high}Ter119^{+}$ and CD41 expression of the bone marrow cells. (L-N) Flow cytometry for the analysis of the percentages of the erythroid ($CD71^{high}Ter119^{+}$), megakaryocytic ($CD41^{+}$), and granulocyte ($Gr1^{+}Mac1^{+}$) lineages of the spleen after treatments. Bar graphs and line graphs depict mean ± SEM; $n = 3$. No significant differences were found via two-way ANOVA (A) or one-way ANOVA (B, C, *E*-N) with a Tukey post-hoc test.

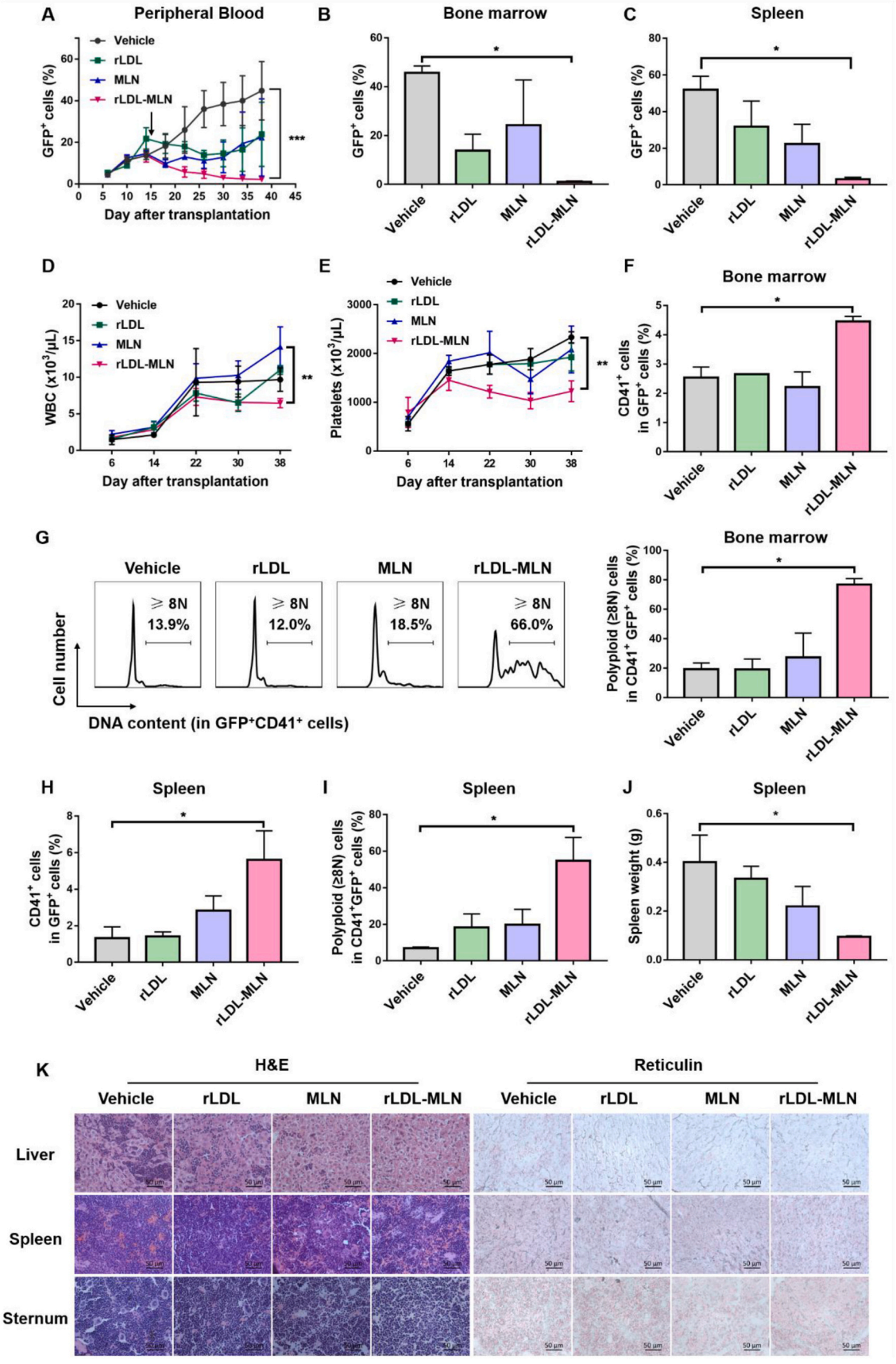

(caption on next page)

Fig. 6. The impacts of rLDL-MLN on reducing the disease burden in the MPLW515L murine myelofibrosis model. MPLW515L recipient mice were intravenously administered with rLDL, MLN, and rLDL-MLN at 0.01 mg/kg or vehicle (tricine) for 3 weeks after transplantation for 15 days. The black arrow indicates the starting time of treatment. GFP^+ cells represent MPLW515L-expressing cells. (A) Flow cytometry for the analysis of the percentage of GFP^+ cells in the peripheral blood. (B) Flow cytometry for the analysis of the percentage of GFP^+ cells in the bone marrow. (C) Flow cytometry for the analysis of the percentage of GFP^+ spleen cells. (D) WBC counts in the peripheral blood. (E) Platelet counts in the peripheral blood. (F) Flow cytometry for the analysis of the percentage of $CD41^+$ GFP^+ cells in the bone marrow. (G) Flow cytometry for the analysis of the polyploidization of the $CD41^+$ GFP^+ cells in the bone marrow. Representative flow cytometry plots (left) and quantification (right) of the DNA content of the $CD41^+$ GFP^+ cells. (H) Flow cytometry for the analysis of the percentage of $CD41^+GFP^+$ cells in the spleen. (I) Flow cytometry for the analysis of the polyploidization of the $CD41^+GFP^+$ cells in the spleen. (J) Spleen weight. (K) Histopathological analysis of tissue sections of bone marrow, liver, and spleen. The tissue samples were hematoxylin-eosin stained and reticulin stained. Images were obtained with a microscope (Axio observer Z1) at a magnification of 400 ×. Scale bars: 50 μm. Bar graphs depict mean ± SEM; $n = 3$. Statistical significance was calculated via two-way ANOVA (A-C) or one-way ANOVA (D-J) with a Dunnett test. $^*P < 0.05$, $^{**}P < 0.01$, $^{***}P < 0.001$.

Table 1
GFP^+ progenitor cell numbers of bone marrow and spleen in the PMF murine model.

Tissue	Population	Vehicle	rLDL	MLN	rLDL-MLN
Bone marrow	**CMP**	**45,216** ± 37,177	**75,490** ± 41,651	**84,258** ± 62,651	**871** ± 630
	GMP	**15,870** ± 10,769	**30,853** ± 24,254	**41,476** ± 29,075	**151** ± 70
	MEP	**36,600** ± 27,281	**75,240** ± 38,030	**68,834** ± 39,143	**1139** ± 957
Spleen	**CMP**	**151,754** ± 38,771	**197,531** ± 130,371	**75,802** ± 41,267	**61** ± 40*
	GMP	**43,853** ± 9370	**97,125** ± 73,689	**68,346** ± 61,661	**4** ± 4**
	MEP	**122,653** ± 36,327	**185,366** ± 141,756	**35,319** ± 17,674	**26** ± 16*

Note: GFP^+ progenitor cells were Lin^- $Scal^-$ $c\text{-}Kit^+$ cells harboring MPLW515L mutation that were gated by flow cytometry analysis. CMP is a common-myeloid progenitor; MEP is a megakaryocyte-erythrocyte progenitor; and GMP is a granulocyte-macrophage progenitor. The values showed the absolute cell numbers of GFP^+ progenitor cells mean ± SEM. Statistical significance was calculated via one-way ANOVA with a Tukey post-hoc test. $^*P < 0.05$, $^{**}P < 0.01$.

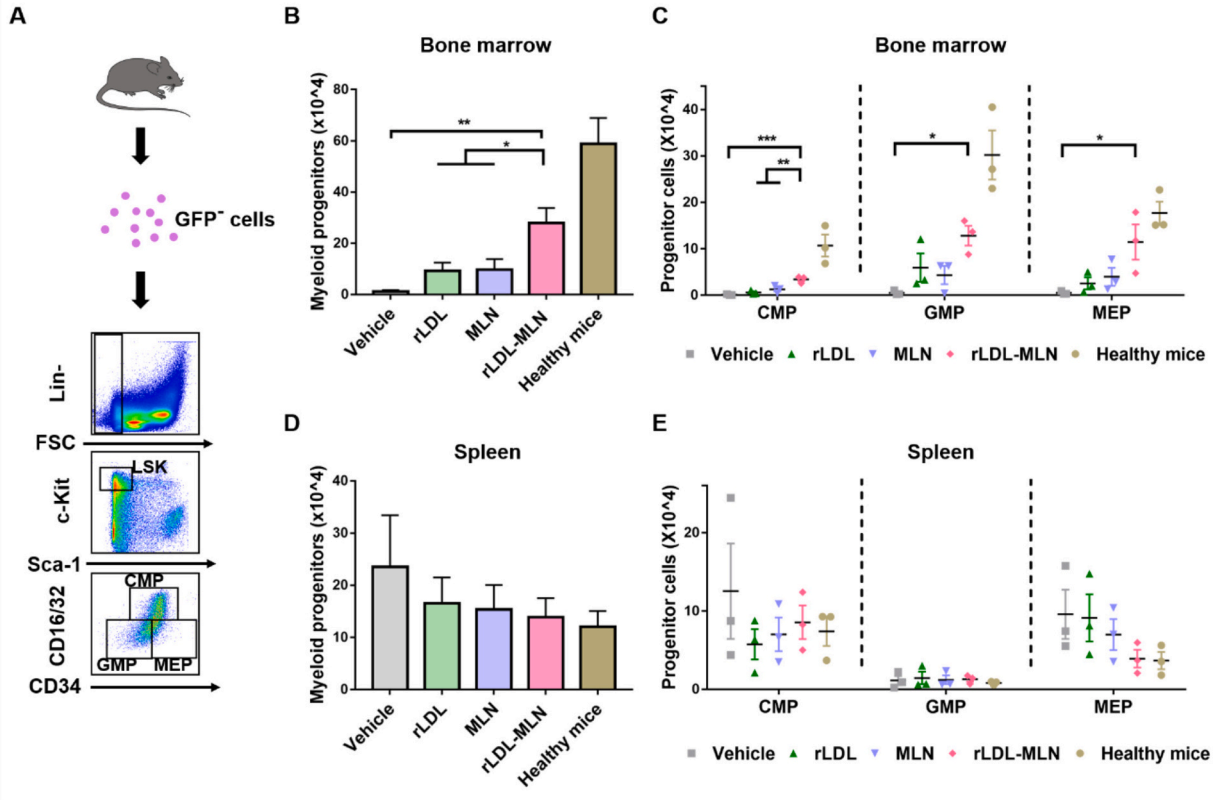

Fig. 7. The role of rLDL-MLN in promoting central hematopoietic recovery and reconstruction in the PMF murine model. MPLW515L recipient mice were intravenously administered with rLDL, MLN, or rLDL-MLN at 0.01 mg/kg or vehicle for 3 weeks after transplantation for 15 days. The GFP^- cells (without MPLW515L mutation) were analyzed by flow cytometry and flowjo software (FlowJo X 10.0.7). Twelve-week-old C57BL/6 N wild-type mice served as the healthy control. (A) Schematic illustration for the evaluation of hematopoietic recovery. (B) Flow cytometry for the analysis of the total myeloid progenitor ($Lin^-Sca\text{-}1^-c\text{-}Kit^+$) cells in the GFP^- bone marrow cells. (C) Flow cytometry for the analysis of the composition of myeloid progenitor cells of GFP^- bone marrow cells. (D) Flow cytometry for the analysis of the total myeloid progenitor cells in the GFP^- spleen cells. (E) Flow cytometry for the analysis of the composition of myeloid progenitor cells of GFP^- spleen cells. Bar graphs depict mean ± SEM; $n = 3$. Statistical significance was calculated via one-way ANOVA (B-E) with a Tukey post-hoc test in PMF mice. $^*P < 0.05$, $^{**}P < 0.01$, $^{***}P < 0.001$.

peripheral hematopoietic organ spleen and blood, rLDL-MLN treatment led to a decrease trend in the numbers of MEP and mature cell lines, which almost restored to the level of healthy mice (Fig. 7E and Table S2). As such, we could conclude that rLDL-MLN plays a crucial role in hematopoietic reconstruction and restoration, providing a promising tool for the treatment of hematopoietic stem cell disease.

3. Discussion

PMF has a relatively lower survival rate than other myeloproliferative neoplasm subtypes due to the expansion and atypical differentiation of megakaryocytic blast cells and myelofibrosis [16]. Several JAK/STAT kinase-targeting small molecule inhibitors have been used for the clinical treatment of PMF. Although the constitutional symptoms, overall survival, and splenomegaly have been alleviated, the mutant allele burden is slightly decreased in myelofibrosis patients [17,18]. Previous studies reported that targeted inhibition of AURKA induced an obvious differentiation of abnormal megakaryocyte blasts and achieved selective treatment of malignant progenitors in the PMF disease [3,5,19]. The AURKA inhibitor MLN8237 has been approved for clinical trial due to its role in significantly inducing polyploidization and the maturation of megakaryocytes. In contrast to JAK2 inhibition, AURKA inhibition resulted in significant reduction of fibrosis and splenomegaly [3]. However, clinical trials showed that some patients did not respond to AURKA inhibitors or were companied with severe adverse effects due to the off-target effect and low bioavailability of AURKA inhibitors [20].

To achieve a better therapeutic effect, artificial drug-delivery platforms were used to optimize the delivery manner of MLN8237, which improved its solubility and intake efficiency [21,22]. For example, a polymeric nanoparticle containing MLN8237 and silver nanoparticles was fabricated for targeted induction of apoptosis of glioblastoma cells both in vitro and in vivo [21]. In addition, a polysaccharide nanovesicle system was developed to deliver MLN8237 to breast cancer cells, resulting in effective AURKA inhibition even at low drug concentrations (0.02–0.04 μM) [22]. However, these polymeric materials are exogenous, which may have immunogenicity and trigger some unknown responses in vivo. As such, the use of an endogenous biological carrier is highly preferred to ameliorate the disease burden and eliminate the undesirable impacts on the patients during treatment process [23,24].

LDL has long been used as a therapeutic nanocarrier to target malignant cells [10,25]. Here, we utilized small molecule inhibitor-loaded rLDL (rLDL-MLN) to dual-target AURKA and malignant PMF blast cells. The nanosized rLDL-MLN was uniform in size and showed targeting capability toward megakaryocytic cells. Our data validated the effectiveness of rLDL-MLN as a targeted therapeutic agent for PMF when considering the following aspects. *i*) rLDL-MLN significantly induced megakaryocytic differentiation of malignant cells and suppressed the proliferation of cells with overexpressed LDLR. The malignant MPLW515L-expressing cells with upregulated LDLR showed significantly increased surface marker expression and polyploidization of megakaryocytes post treatment with rLDL-MLN when compared to equivalent free MLN. Meanwhile, there were less MPLW515L mutation progenitor cells in the rLDL-MLN group than that in the control groups. Besides, consistent results were observed in the hematological organs, bone marrow, and spleen of the rLDL-MLN treated-MPLW515L PMF murine model. Notably, the rLDL-MLN-treated mice exhibited almost cleared blasts, whereas the MLN-treated mice still suffered from general PMF symptoms. *ii*) rLDL-MLN remarkably ameliorated disease burden and almost cured the PMF mice even at a low dosage of 0.01 mg/kg. It not only reduced the blast cells but also induced the rest blast cells to become more mature megakaryocytes with less malignant characteristics. *iii*) At the effective dosage, rLDL-MLN did not show evident toxic effects on the liver and hematopoietic tissues of healthy mice. Besides, the composition of the peripheral blood and myeloid cells maintained the same status as the healthy one. *iv*) rLDL-MLM treatment promoted hematopoietic recovery and reconstruction of PMF mice, where the progenitor cell numbers and the myeloid cells increased to a normal level post rLDL-MLN treatment.

As a naturally occurring biological carrier, LDL has a variety of advantages, including reduced immunogenicity, low side effects, long-circulating time, high loading capacity, and LDLR-targeting capability [26]. In this study, the rLDL-MLN nanoparticles were constructed from native LDL, and, thus, they inherited all the merits of LDL. Taking advantage of LDLR-mediated endocytosis, LDL-based drug delivery systems can effectively deliver therapeutic agents to specific sites in vivo, such as the liver [27], the brain [11], and some malignant cancer tissues [10]. In addition to its targeting capability, our findings showed the rLDL imposed an inhibitory effect on malignant progenitor cells. Notably, rLDL-MLN could induce the remaining malignant cell blasts to revert to more mature megakaryocytes. Besides, rLDL-MLN facilitated hematopoietic recovery and made the treated PMF mice exhibit a normal hematopoietic progenitor differentiation pattern that was similar to wild-type mice. Such a feature is desired as it can rescue the hematopoietic disorders and myelofibrosis of PMF disease. It is speculated that rLDL-MLN is able to improve the hematopoietic microenvironment and inflammatory status by restoring the differentiation degree of megakaryocytes.

The limitation of this study might be the scarce supply of LDL. Until now, no LDL-based therapeutic agents are applied in clinical trials. One possible reason lies in the limited availability as most LDL is isolated from blood, and it is difficult to obtain large quantities for clinical practice. In addition, although the hydrophobic components in the core of LDL was removed to affect lipid metabolism, further studies regarding its impacts on hepatocytes still need to be performed prior to possible clinical trials.

4. Conclusion

In summary, we developed an effective LDL-based nanodrug rLDL-MLN for the treatment of the stem cell/progenitor-derived myelofibrosis neoplasm disease, PMF. The rLDL-MLN nanoparticles showed dual-targeting capability toward specific malignant cells and AURKA, which not only inhibited the proliferation of malignant cells but also induced the differentiation to mature megakaryocytes, including the elevation of megakaryocytic surface marker expression and polyploidization degree. In vivo evaluation demonstrated that rLDL-MLN exhibited excellent differentiation therapeutic effect in the PMF murine model, where the malignant cells in the hematological organs were nearly cleared and the rest blasts were reverted to poorly differentiated mature cells. Besides, rLDL-MLN is conducive to the hematological restoration and reconstruction, whereas free MLN8237 did not elicit such an effect at the same dose, holding great promise for clinical treatment of PMF disease.

5. Materials and methods

5.1. rLDL-MLN nanoparticle

The rLDL-MLN nanoparticles were fabricated according to our previous report [10,28]. Briefly, native LDL particles (LEEBIO, 360–10, USA) (1 mg) in water (200 μL) were vortexed with potato starch (12.5 mg), followed by freeze-drying and lipid extraction with heptane three times. Next, a mixture of fatty acids in toluene (lauric acid = 8 mg/mL, stearic acid = 2 mg/mL; 100 μL) and MLN in DMSO (2.6 mg/mL; 2.5 μL) were premixed and added to the mixture of LDL and starch. As a control, a mixture of fatty acids at the same concentration and volume but without MLN was also used for LDL reconstitution. After incubation at −20 °C for 20 min, the mixture was placed in an ice bath, followed by solvent evaporation under an argon atmosphere. To release the rLDL particles, the dried mixture was dispersed in the tricine buffer (10 mM, pH = 8.4; 300 μL) at 4 °C for 18 h, followed by centrifugation at 2000 rpm for 10 min. The supernatant was subjected to additional two rounds

of centrifugation (10,000 rpm, 10 min) for further purification. After passing through a 0.22-μm sterile filter (Millipore), the rLDL particles were stored at 4 °C for subsequent use. The rLDL particles with and without MLN were denoted as rLDL-MLN and rLDL, respectively. To quantify the concentration of MLN and rLDL-MLN, the nanoparticles were disassembled and extracted with methanol under ultrasonication, followed by centrifugation at 10000 rpm for 5 min. The supernatant of both samples was measured by a UV/vis spectrometer (Shimadzu, UV-2600). The concentration of MLN was then determined by referring to the corresponding calibration curve (Fig. S1B). The morphology of all rLDL was characterized by transmission electron microscopy (TEM, Tecnai, G2 F20, 200 kV). Prior to TEM characterization, the samples were negatively stained with 2 wt% uranyl acetate. The encapsulation efficiency of MLN in rLDL-MLN was calculated using the following formula:

$$\text{Encapsulation efficiency} = \frac{\text{Weight of MLN in nanoparticles}}{\text{Weight of the feeding MLN}} \times 100\% = \frac{35\ \mu\text{M} \times 300\ \mu\text{L}}{5\ \text{mM} \times 2.5\ \mu\text{L}} \times 100\% = 84\%$$

5.2. Cell Culture

5.2.1. Cell lines

HEL cells and K562 cells were obtained from the National Collection of Authenticated Cell Cultures (NCACC, China). MEG-01 cells were obtained from the Cell Resource Center, Peking Union Medical College (CRC/PUMC, China). 6133/MPLW515L cells, SET-2 cells, and plat-E cells were obtained from Department of Medicine, Division of Hematology and Oncology, Northwestern University.

HEL, K562, and 6133/MPLW515L cells were cultured in RPMI Medium 1640 (Thermo Fisher Scientific, 31,800,022) supplemented with 10% FBS and 1% antibiotics (Gibco, 15,140,122), while SET-2 and MEG-01 cells were cultured in RPMI Medium 1640 supplemented with 20% FBS and 1% antibiotics. Plat-E cells were cultured in DMEM (Thermo Fisher Scientific, 12,800,017) supplemented with 10% FBS and 1% antibiotics. All the cells are cultured in a humidified atmosphere at 37 °C with 5% CO_2.

5.2.2. HSPC cells

Mouse primary bone marrow cells were isolated from the bone marrow of healthy C57BL/6 N female mice (6 weeks) by anti-c-Kit$^+$ MicroBeads (Miltenyi Biotec, 130–091-224). Mouse bone marrow progenitor cells were cultured in StemSpan (Stemcell technologies, 09650) supplemented with 10 ng/mL mouse IL-3 (PeproTech, 213–13), 10 ng/mL human IL-6 (PeproTech, 200–06), and 40 ng/mL mouse SCF (PeproTech, 315–02), along with 20 μg/mL human LDL (LeeBio, 360–10). To observe megakaryocyte differentiation, c-Kit$^+$ cells were cultured in RPMI Medium 1640 supplemented with 10% FBS and 1% antibiotics for 48 h.

5.3. Retroviral transduction

Retrovirus Migr1-GFP-MPLW515L [29] plasmid was obtained from the Division of Hematology and Oncology. For the package of retroviral experiments, plat-E cells (5×10^6) were seeded in a 10-cm dish the day before transfection and then transfected with Migr1-GFP-MPLW515L plasmid using DNA Transfection Reagent (Roche, 6,365,779,001) following the manufacturer's protocols. After transfection for 48 h, the viral supernatant was collected. 1 mL of viral supernatant was mixed with 2×10^6 of mouse bone marrow progenitor cells companied with 8 μg/ml polybrene (Sigma, TR-1003-G) and then centrifuged at 2500 rpm for 90 min at 32 °C. Spinoculation was performed twice after c-Kit$^+$ cells were extracted and cultured for 24 h.

5.4. In vitro proliferation and differentiation assays

Cells were plated in 24-well tissue culture-treated plates in 1.5 mL media with tricine or other inhibitory agents for various periods of time. At the end of incubation, proliferation viability was assessed using trypan blue staining (Solarbio, C0040) or flow cytometry (BD AriaIII). Cell surface markers CD41, CD42, DNA content, and annexin V were evaluated by flow cytometry. The IC50 was calculated with non-linear regression analysis of GraphPad Prism 7.0 software.

Primary mouse bone marrow cells were incubated with tricine or inhibitory agents in the presence of 10 ng/mL mouse SCF after retroviral transduction. At the end of incubation, cell counts were assessed using trypan blue staining. The cell surface markers, DNA contents, and annexin V were evaluated by flow cytometry.

5.5. CFU assays

Assays of colony-forming unit-megakaryocyte (CFU-MK) and colony-forming unit-myeloid (CFU-myeloid) cells were performed on MPLW515L-expressing mouse c-Kit$^+$ cells. For CFU-MK assay, 10,000 MPLW515L-expressing mouse c-Kit$^+$ cells were seeded in Megacult-C medium (Stemcell Technologies) supplemented with 10 ng/mL mouse IL-3, 10 ng/mL human IL-6, and 50 ng/mL of mouse THPO and cultured in the presence of tricine or chemical inhibitors for 7–9 days. For CFU-myeloid assay, 6000 MPLW515L overexpressing mouse c-Kit$^+$ cells were seeded in MethoCult medium (Stemcell Technologies) supplemented with 10 ng/mL mouse IL-3, 10 ng/mL human IL-6, 10 ng/mL mouse SCF and cultured in the presence of tricine or inhibitory agents for 9 days. Slides of megakaryocyte cultures were fixed with acetone and then stained with substrates of acetylcholinesterase according to the manufacturer's instructions followed by colony counting. For the CFU-myeloid assay, CFU-E, CFU-GEMM, and CFU-G/M were counted on day 9 according to the manufacturer's instructions.

5.6. Animal experiments

C57BL/6 N mice were obtained from Charles River Laboratories. For the MPLW515L murine model, C57BL/6 N bone marrow progenitor cells were enriched by c-Kit$^+$ selection and cultured overnight. On the next day, the cells were transduced with human MPLW515L retrovirus. On the third day, recipient C57BL/6 N mice were transplanted with transduced bone marrow cells after lethal irradiation with a dose of 950 rads and transplanted with 0.3×10^6 GFP$^+$ cells. Recipient mice developed leukocytosis, polycythemia, and thrombocytosis in 2–3 weeks. In terms of drug studies, mice were randomized to different treatment groups based on the level of GFP$^+$ cancer cells in the peripheral blood. rLDL-MLN, MLN, and rLDL at a dose of 0.01 mg/kg or the tricine vehicle were injected to transplant recipients of MPLW515L cells by intravenous injection every 3 days. Notably, the experimental design was blinded in such a way that the researcher assessing the outcome was unaware of the treatment groups. Female mice between 8 and 12 weeks of age were used for all transplant studies.

5.7. Complete blood counts

Murine blood (20 μL) was collected from the tail vein in EDTA-coated tubes and analyzed by an automated hematology analyzer (MEK-6410C, Japan).

5.8. Histopathology

Tissues were fixed in 4% paraformaldehyde, embedded in paraffin, and stained with hematoxylin and eosin (Solarbio, G1120) to assess cancer infiltration or with a Reticulin stain kit (Solarbio, G3525) to assess fibrosis following the manufacturer's instructions. Blood smears were fixed in methanol and stained in Giemsa solutions (Solarbio,

G1015) according to the manufacturer's instructions. Images of histological slides were obtained on a ZEISS inverted microscopy (Zeiss Axio observer Z1, Germany) equipped with a color digital camera (Leica, Germany). The images were analyzed with Zen blue 2.3 software.

5.9. Immunohistochemistry

LDLR expression was determined by immunohistochemistry using 5-μm-thick sections that were stained using a monoclonal anti-LDLR (diluted 1:100) produced in rabbit (Abcam, ab52818). The slices were dewaxed with xylene and rehydrated in ethanol. The endogenous peroxidase activity was blocked by hydrogen peroxide, and the nonspecific antigens were blocked by 5% BSA/TBST. After overnight incubation with primary antibodies at 4 °C, the sections were treated with ready-to-use biotin-labeled goat anti-rabbit IgG polymer (Abcam, ab6721), followed by horseradish peroxidase-conjugated streptavidin, enabling positive signal detection with DAB substrate (Solarbio, DA1016).

5.10. Flow cytometry

For in vitro differentiation experiments, surface marker staining for human CD41 (BD Pharmingen, 559,777) or mouse CD41 (eBioscience, 25–0411-82) and CD42b (BD Pharmingen, 558,819) was performed by incubation for 15 min in PBS at 4°Cin dark. For in vivo differentiation experiments, bone marrow cells were flushed from hind leg bones with PBS, and spleen cells were prepared by pressing tissue through a cell strainer. After lysing with red blood cell lysis solution, single-cell suspensions were prepared by resuspending the cells in PBS with 0.5% BSA and 2 mM EDTA. Surface marker staining for mouse CD41, Ter119 (BD Pharmingen, 557,909), CD71 (BD Pharmingen, 553,267), CD11b (BD Pharmingen, 557,397), and Mac1 (Invitrogen, 17–5931-81) were performed similarly. For mouse hematopoietic progenitor analysis, bone marrow cells and splenocytes from the murine myelofibrosis model were stained with antibodies against c-Kit (eBioscience, 47–1171-82), Sca-1 (eBioscience, 12–5981-81), CD34 (BD Pharmingen, 560,230), and FcγR (eBioscience, 25–0161-81) to label stem and myeloid progenitor populations, including LSK, CMP, GMP, and MEP. For annexin V staining, cells were incubated with an annexin V antibody (BD, 550474) in a binding buffer for 15 min at room temperature in dark. For DNA content analysis, human or mouse cells were incubated with Hoechst 33342 at 37 °C in dark for 40 min. The cells were gated based on cell viability or GFP positivity. For differentiation analysis of cell lines, the minimum of the number of events is 20,000 events. For differentiation analysis of progenitor cells, the minimum of the number of events is 2,000,000 events. For the analysis of GFP^+ cell percentages of the peripheral blood, the minimum of the number of events is 10,000 events. Data were analyzed using FlowJo X 10.0.7 software.

5.11. Quantitative PCR

Total RNAs were isolated from cell lines or bone marrow cells or spleen cells in MPLW515L transduced mice according to the manufacturer's instructions (Roche, 15,596,018). After reverse transcription with M-MLV Reverse Transcriptase (Promega, M1701). Quantitative PCR was performed with ABI Quant Studio 6 Flex and *Ldlr* gene; *Tgf-β* gene expression was analyzed; and *β*-actin served as control.

5.12. Western blot assay

HEL cells or murine bone marrow cells were lysed in RIPA buffer (10 × MOPS, 2 mM EGTA, 5 mM EDTA, 30 mM NaF, 60 mM β-glycerophosphate, 20 mM Sodium pyrophosphate, 1% NP-40) supplemented with protease inhibitors (Roche) and phosphatase inhibitor (1 mM Na_3VO_4). Proteins were separated by SDS-PAGE and transferred onto a PVDF membrane. Membranes were blotted with antibodies detecting phospho-AURKA (Cell Signaling, 3079), AURKA (GeneTex, GTX13824), and HSC70 (Santa Cruz Biotechnology, SC-7298).

5.13. Statistics

For quantitative assays, treatment groups were reported as mean ± SEM and compared using the unpaired two-sided Student's *t*-test. When multiple comparisons were necessary, one-way or two-way analysis of variance with Tukey post-test was used. For in vivo evaluation, one-way or two-way analysis of variance with the Dunnett-test was used. Statistical significance was established at P less than or equal to 0.05, labeled as * $P \leq 0.05$, ** $P \leq 0.01$, *** $P \leq 0.001$, and **** $P \leq 0.0001$. All analyses were performed using GraphPad Prism 7.0 (GraphPad Software).

Author contributions

B.H. designed research, performed experiments, analyzed data, and wrote the manuscript; C.W. and L.T. designed, synthesized, and characterized rLDL-MLN; F.W., H.W. and C.F. offered technical support of the MPLW515L murine model; J.L. and C.X. offered technical support of the flow cytometry and paraffin slicing machine; C.Z. supervised the preparation of rLDL-MLN and revised the manuscript; Q.Y. designed research and revised the manuscript.

Declaration of Competing Interest

The authors declare no competing interests.

Data availability

All data are available in the main text or the supplementary materials.

Acknowledgements

We thank John D. Crispino for the plasmids of MPLW515L and SET-2 and 6133/MPLW515L cells. This work was supported by the Natural Science Foundation of Beijing Municipality (2202021) and National Natural Science Foundation of China (22072005, 21773015).

Appendix A. Supplementary data

Supplementary data to this article can be found online at https://doi.org/10.1016/j.jconrel.2023.03.024.

References

[1] A. Tefferi, Primary myelofibrosis: 2021 update on diagnosis, risk-stratification and management, Am. J. Hematol. 96 (2021) 145–162.
[2] A. Karagianni, K. Ravid, Myeloproliferative disorders and their effects on bone homeostasis: the role of megakaryocytes, Blood. 139 (2022) 3127–3137.
[3] Q. Jeremy Wen, Q. Yang, B. Goldenson, S. Malinge, T. Lasho, R.K. Schneider, et al., Targeting megakaryocytic-induced fibrosis in myeloproliferative neoplasms by AURKA inhibition, Nat. Med. 21 (2015) 1473–1480.
[4] L. Pieri, C. Paoli, U. Arena, F. Marra, F. Mori, M. Zucchini, et al., Safety and efficacy of ruxolitinib in splanchnic vein thrombosis associated with myeloproliferative neoplasms, Am. J. Hematol. 92 (2017) 187–195.
[5] Q. Wen, B. Goldenson, S.J. Silver, M. Schenone, V. Dancik, Z. Huang, et al., Integrative screening approach identifies regulators of polyploidization and targets for acute megakaryocytic leukemia, Cell. 150 (2012) 575.
[6] K. Range, Y.A. Moser, Molecular pathways: induction of polyploidy as a novel differentiation therapy for leukemia, Clin. Cancer Res. 23 (2012) 1–7.
[7] J. Den Hollander, S. Rimpi, J.R. Doherty, M. Rudelius, A. Buck, A. Hoellein, et al., Aurora kinases A and B are up-regulated by Myc and are essential for maintenance of the malignant state, Blood. 116 (2010) 1498–1505.
[8] N. Gangat, C. Marinaccio, R. Swords, J.M. Watts, S. Gurbuxani, A. Rademaker, et al., Aurora kinase a inhibition provides clinical benefit, normalizes megakaryocytes, and reduces bone marrow fibrosis in patients with myelofibrosis: a phase I trial, Clin. Cancer Res. 25 (2019) 4898–4906.

[9] M. Masquelier, S. Vitols, C. Peterson, Low-density lipoprotein as a carrier of antitumoral drugs: in vivo fate of drug-human low-density lipoprotein complexes in mice, Cancer Res. 46 (1986) 3842–3847.
[10] C. Zhu, P. Pradhan, D. Huo, J. Xue, S. Shen, K. Roy, et al., Reconstitution of low-density lipoproteins with fatty acids for the targeted delivery of drugs into cancer cells, Angew. Chem. Int. Ed. Eng. 56 (2017) 10399–10402.
[11] R.S. Mulik, C. Bing, M. Ladouceur-Wodzak, I. Munaweera, R. Chopra, I.R. Corbin, Localized delivery of low-density lipoprotein docosahexaenoic acid nanoparticles to the rat brain using focused ultrasound, Biomaterials. 83 (2016) 257.
[12] M. Nikanjam, E.A. Blakely, K.A. Bjornstad, X. Shu, T.F. Budinger, T.M. Forte, Synthetic nano-low density lipoprotein as targeted drug delivery vehicle for glioblastoma multiforme, Int. J. Pharm. 328 (2007) 86–94.
[13] S. Vitols, M. Björkholm, G. Gahrton, C. Peterson, Hypocholesterolaemia in malignancy due to elevated low-density-lipoprotein-receptor activity in tumour cells: evidence from studies in patients with leukaemia, Lancet (London, England) 2 (1985) 1150–1154.
[14] A. Tefferi, P. Guglielmelli, D.R. Larson, C. Finke, E.A. Wassie, L. Pieri, et al., Long-term survival and blast transformation in molecularly annotated essential thrombocythemia, polycythemia vera, and myelofibrosis, Blood. 124 (2014) 2507–2513.
[15] H. Quentmeier, R.A.F. MacLeod, M. Zaborski, H.G. Drexler, JAK2 V617F tyrosine kinase mutation in cell lines derived from myeloproliferative disorders, Leuk. 203 (20) (2006) 471–476.
[16] E. Rumi, M. Cazzola, Diagnosis, risk stratification, and response evaluation in classical myeloproliferative neoplasms, Blood. 129 (2017) 680.
[17] S. Verstovsek, R.A. Mesa, J. Gotlib, R.S. Levy, V. Gupta, J.F. DiPersio, et al., A double-blind, placebo-controlled trial of ruxolitinib for myelofibrosis, N. Engl. J. Med. 366 (2012) 799–807.
[18] M. Kleppe, M. Kwak, P. Koppikar, M. Riester, M. Keller, L. Bastian, et al., JAK-STAT pathway activation in malignant and nonmalignant cells contributes to MPN pathogenesis and therapeutic response, Cancer Discov. 5 (2015) 316–331.
[19] B. Goldenson, G. Kirsammer, M.J. Stankiewicz, Q.J. Wen, J.D. Crispino, Aurora kinase A is required for hematopoiesis but is dispensable for murine megakaryocyte endomitosis and differentiation, Blood. 125 (2015) 2141–2150.
[20] R.T. Piszczatowski, U. Steidl, Aurora kinase A inhibition: a mega-hit for myelofibrosis therapy? Clin. Cancer Res. 25 (2019) 4868.
[21] E. Locatelli, M. Naddaka, C. Uboldi, G. Loudos, E. Fragogeorgi, V. Molinari, et al., Targeted delivery of silver nanoparticles and alisertib: in vitro and in vivo synergistic effect against glioblastoma, Nanomedicine (London) 9 (2014) 839–849.
[22] S. Inchanalkar, N.U. Deshpande, V. Kasherwal, M. Jayakannan, N. Balasubramanian, Polymer nanovesicle-mediated delivery of MLN8237 preferentially inhibits aurora kinase a to target RalA and anchorage-independent growth in breast cancer cells, Mol. Pharm. 15 (2018) 3046–3059.
[23] D. Rosenblum, N. Joshi, W. Tao, J.M. Karp, D. Peer, Progress and challenges towards targeted delivery of cancer therapeutics, Nat. Commun. 9 (2018).
[24] M. Bar-Zeev, Y.D. Livney, Y.G. Assaraf, Targeted nanomedicine for cancer therapeutics: towards precision medicine overcoming drug resistance, Drug Resist. Updat. 31 (2017) 15–30.
[25] M. Nikanjam, A.R. Gibbs, C.A. Hunt, T.F. Budinger, T.M. Forte, Synthetic nano-LDL with paclitaxel oleate as a targeted drug delivery vehicle for glioblastoma multiforme, J. Control. Release 124 (2007) 163–171.
[26] C. Zhu, Y. Xia, Biomimetics: reconstitution of low-density lipoprotein for targeted drug delivery and related theranostic applications, Chem. Soc. Rev. 46 (2017) 7668–7682.
[27] X. Wen, L. Reynolds, R.S. Mulik, S.Y. Kim, T. Van Treuren, L.H. Nguyen, et al., Hepatic arterial infusion of low-density lipoprotein docosahexaenoic acid nanoparticles selectively disrupts redox balance in hepatoma cells and reduces growth of orthotopic liver tumors in rats, Gastroenterology. 150 (2016) 488–498.
[28] C. Wang, X. Zhao, H. Jiang, J. Wang, W. Zhong, K. Xue, et al., Transporting mitochondrion-targeting photosensitizers into cancer cells by low-density lipoproteins for fluorescence-feedback photodynamic therapy, Nanoscale. 13 (2021) 1195–1205.
[29] K. Hussein, O. Bock, K. Theophile, K. Schulz-Bischof, A. Porwit, J. Schlue, et al., MPLW515L mutation in acute megakaryoblastic leukaemia, Leuk. 2009 235. 23 [1]852–855.